Biophysical Journal, Volume *115*

Supplemental Information

Nonlinear Elasticity of the ECM Fibers Facilitates Efficient Intercellular Communication

Ran S. Sopher, Hanan Tokash, Sari Natan, Mirit Sharabi, Ortal Shelah, Oren Tchaicheeyan, and Ayelet Lesman

Nonlinear elasticity of the ECM fibers facilitates efficient inter-cellular communication

RS Sopher, H Tokash, S Natan, M Sharabi, O Shelah, O Tchaicheeyan, A Lesman

Supplemental Information

Derivation and validation of the mechanical properties assigned to the network fibers - Figure S1 Figure S2

The mechanical properties assigned to the fibers contained in the ECM were derived from the simulated macroscale properties of the network, which were juxtaposed with previous experimental findings of the bulk response of collagen gels to uniaxial loading. In detail, a network consisting of truss elements of diameter of 200 nm (which is within the range reported by (15) for the diameter of collagen fibers), and of rectangular shape (length: 535 μm, width: 229 μm), was created as described in Section **Error! Reference source not found.**. The individual fibers were modeled as demonstrating all types of mechanical behavior listed in Section **Error! Reference source not found.**, while the reference elastic modulus (E_{ref}) was initially set at a random value. The bottom edge of this virtual specimen was fixed for all translations and rotations. Uniaxial tension was introduced by applying maximum displacement of 100 μm to the top edge of the specimen. The nominal strain applied to the specimen was continuously calculated by dividing the length change of the rectangle in the vertical axis (*i.e.*, the vertical displacement occurring at the top edge) by the reference, undeformed length (*i.e.*, the initial length of the rectangle). The nominal stress applied to the specimen was calculated as the sum of the vertical components of all reaction forces occurring at the upper edge of the rectangle, divided by the axial cross-sectional area of the specimen (the width of the rectangle multiplied by the 'depth' of the specimen, *i.e.* the fiber diameter of 200 nm). The calculated stresses were plotted against the calculated strains, and the resulted curve, which demonstrated the macroscale stiffness of the simulated fibrous material, was juxtaposed with the reported mechanical behavior of collagen gel 2.4 mg/ml subjected to uniaxial tension, as measured using a rheometer (12) (Figure S1). The value of E_{ref} assigned to the individual fibers was iteratively adjusted until reaching satisfactory resemblance between the curves (a process similar to that described by (1)), and was ultimately set at 11.5 kPa.

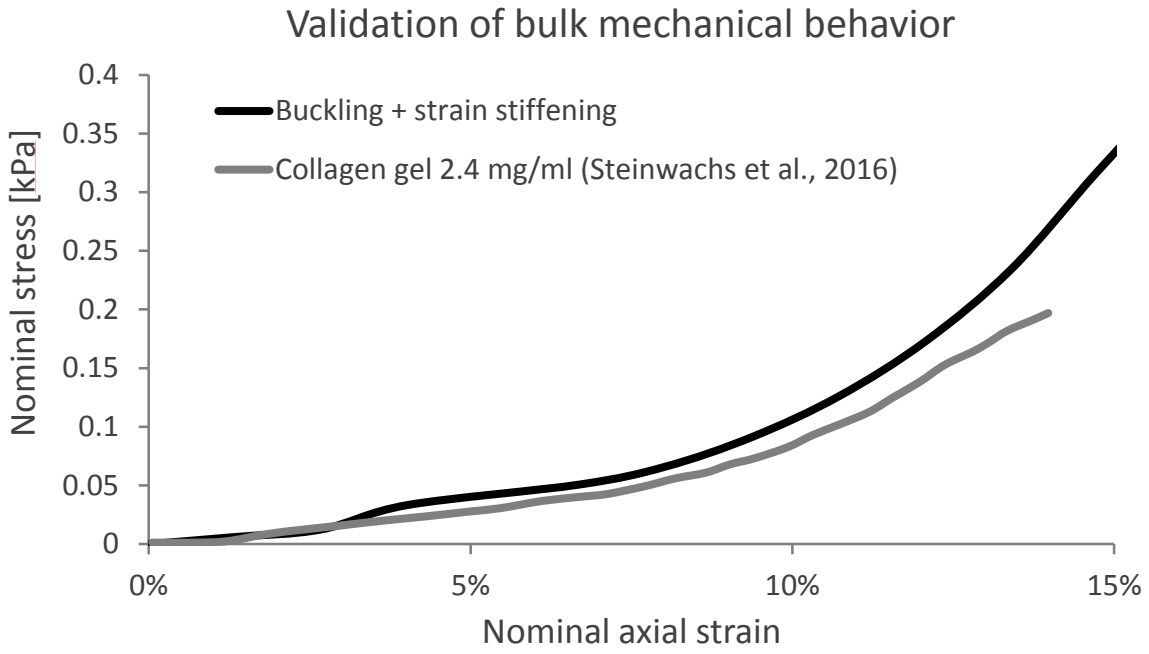

Figure S1: Stress-strain curve demonstrating the bulk mechanical behavior of the simulated fibrous network (when assuming fiber diameter of 200 nm, tension-stiffening of the individual fibers and E_{ref}=11.5 kPa) when subjected to uniaxial tension, juxtaposed with an equivalent curve derived experimentally for collagen gel 2.4 mg/ml (12).

The stress-strain relationships demonstrated by the simulated bulk material, as derived from the aforementioned analysis when assuming each of the four types of fiber mechanical behavior listed in Section **Error! Reference source not found.** and implementing the aforementioned value of E_{ref}, are shown in Figure S2a. When assuming tension-stiffening behavior of the individual fibers (material model iii in Section **Error! Reference source not found.**), the bulk materials was the stiffest, followed by fibers demonstrating both tension-stiffening and compression-buckling (material model iv). In other words, the elevated resistance of the fibers contained in the network to tension resulted in an increased tension-stiffness of the bulk material. When assuming fiber compression-buckling alone (material model ii), the bulk material was slightly softer than when assuming linear elasticity (material model i in Section **Error! Reference source not found.**) (Figure S2a). This is attributable to the decreased resistance of the fibers subjected to compression loading (particularly those aligned horizontally, *i.e.* along the width of the specimen, which is subjected to transverse strain) to such compression.

The Poisson's ratio of the simulated material was also calculated when assuming all types of fiber mechanical behavior listed in Section **Error! Reference source not found.**, by dividing the nominal strain along the width of the rectangular specimen (transverse strain) by the nominal strain along its length (axial strain), and multiplying the result by -1. When assuming linear-elastic behavior of the individual fibers, Poisson's ratio was nearly constant at 0.4-0.5 (Figure S2b). When modeling the fibers as bucklable, increasing axial strain

resulted in a gradual increase in the Poisson's ratio, which is in agreement with previous findings (26). Tension-stiffening of the individual fibers resulted in the Poisson's ratio of the simulated bulk material exceeding 1 (Figure S2b), which is in agreement with a previous computational model (35).

Pure shear was also exerted to the virtual specimen by applying horizontal displacement to the top edge of the rectangle. The engineering shear strain applied to the specimen was continuously calculated as the change in angle between the horizontal and vertical edges of the rectangle. The engineering shear stress was calculated as the sum of the horizontal components of all reaction forces occurring at the upper edge of the rectangle, divided by the axial cross-sectional area of the specimen. The shear modulus of the bulk material was subsequently estimated as the fraction of the shear stress to the shear strain applied to the specimen. The shear modulus was then plotted against the engineering shear strain (Figure S2c). Tension-stiffening of the individual fibers resulted in the shear modulus increasing with the shear strain. Fiber compression-buckling resulted in the bulk shear modulus being considerably smaller (Figure S2c), which is attributable to a decreased resistance of the fibers to compression.

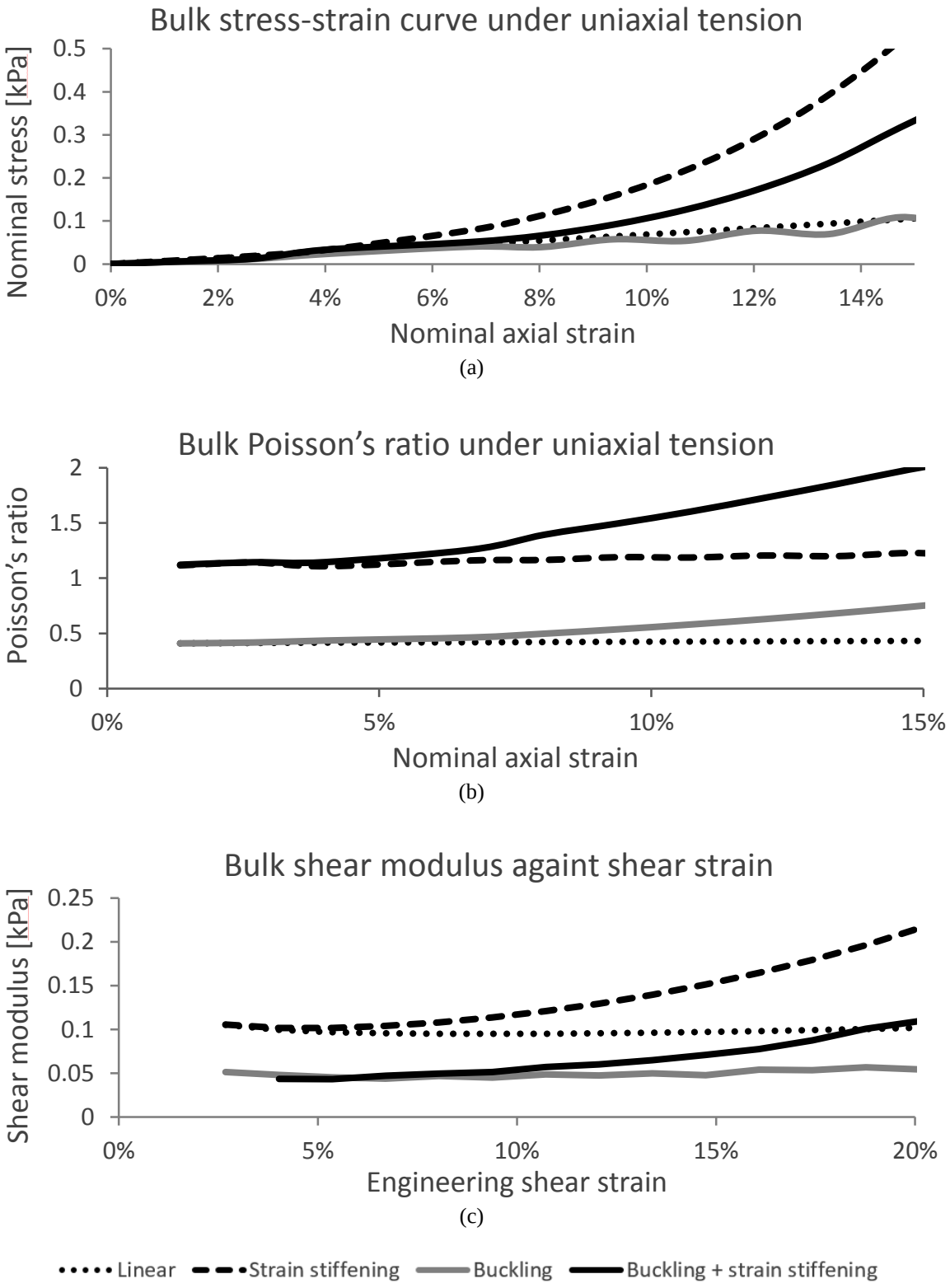

Figure S2: The bulk mechanical behavior of the simulated fibrous network (when assuming fiber diameter of 200 nm and E_{ref}=11.5 kPa) for four types of mechanical behavior of the individual fibers (**Error! Reference source not found.**c): (a) stress-strain relationship under uniaxial tension; (b) Poisson's ratio under uniaxial tension; (c) shear modulus against engineering shear strain.

The decay of displacements in the vicinity of a single contracting cell - Figure S3

To validate the model we analyzed the decay of displacements induced by the contraction of a single cell for the four types of fiber mechanical behavior (Section **Error! Reference source not found.**). The radial displacements occurring in the ECM were plotted against the distance from the cell center and fit to a power function (see details in the figure caption below). For linear-elastic fibers we found that a decay coefficient of 0.90, which resembles the value of 1 predicated by linear-elastic theory in 2D systems (54). The decay of displacments in the vicinity of the contracting cell was found to be slower when embbeded in compression-buckling fibers (decay coefficient of 0.56), which is in line with the findings of previous experimental, analytical and computational studies (21, 25, 26).

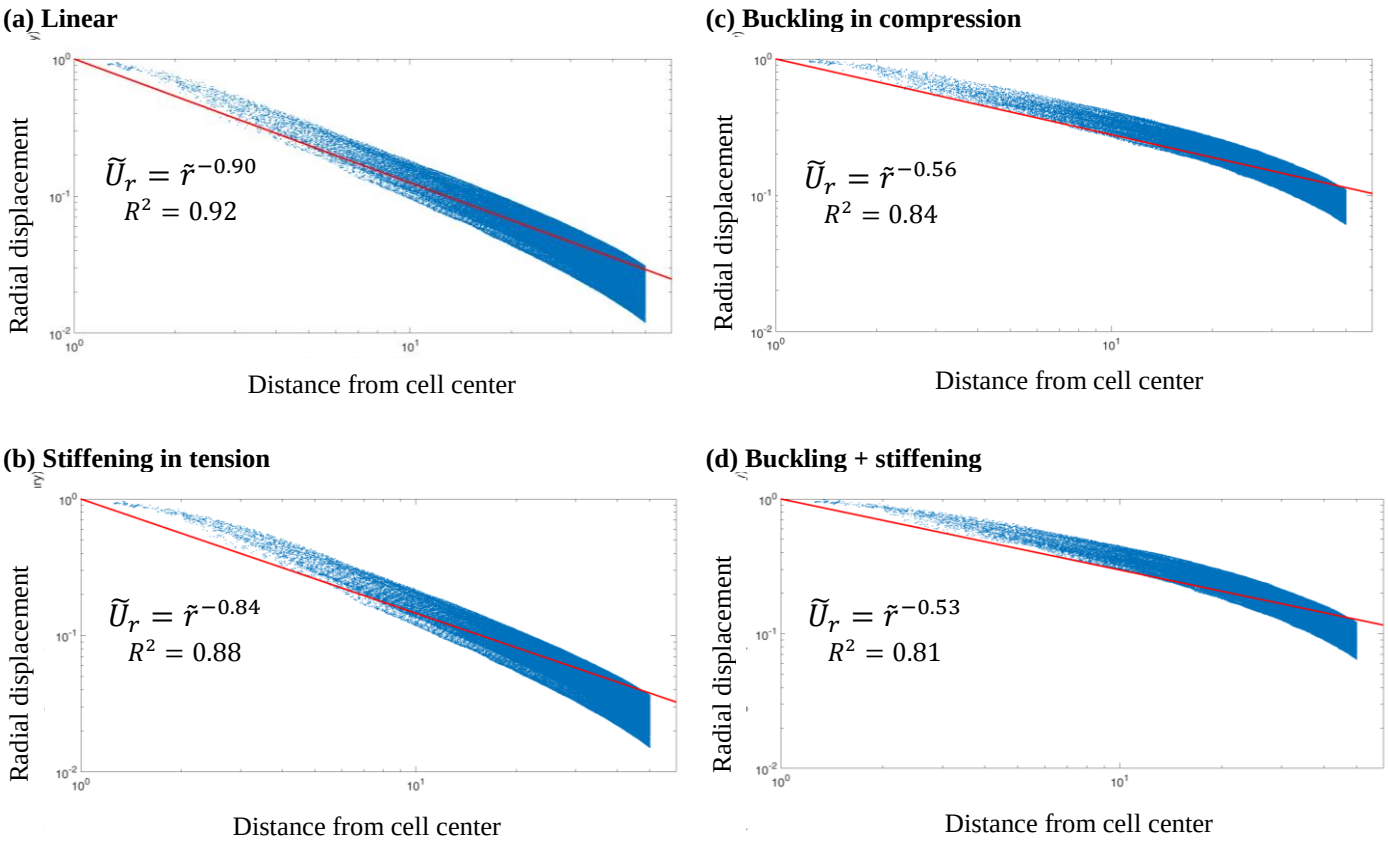

Figure S3: Propagation of displacements occurring in the ECM due to contraction of a single cell embedded in networks with four different types of mechanical behavior (**Error! Reference source not found.**c), for 25% cell contraction. Specifically, each plot shows the radial components of the displacements (normalized according to the radial displacement of the cell boundaries) of the centers of the fibers forming the model network (up to a distance equivalent to the midway between the cell center and the network boundaries) as a function of the distance from the center of the contracting cell (normalized according to the cell radius) (blue dots) (note the logarithmic scales of both axes). The displacements were fit to a $U=r^{-n}$ function (red lines) according to the least-square method, where U is the normalized displacement and r is the normalized distance from the cell center.

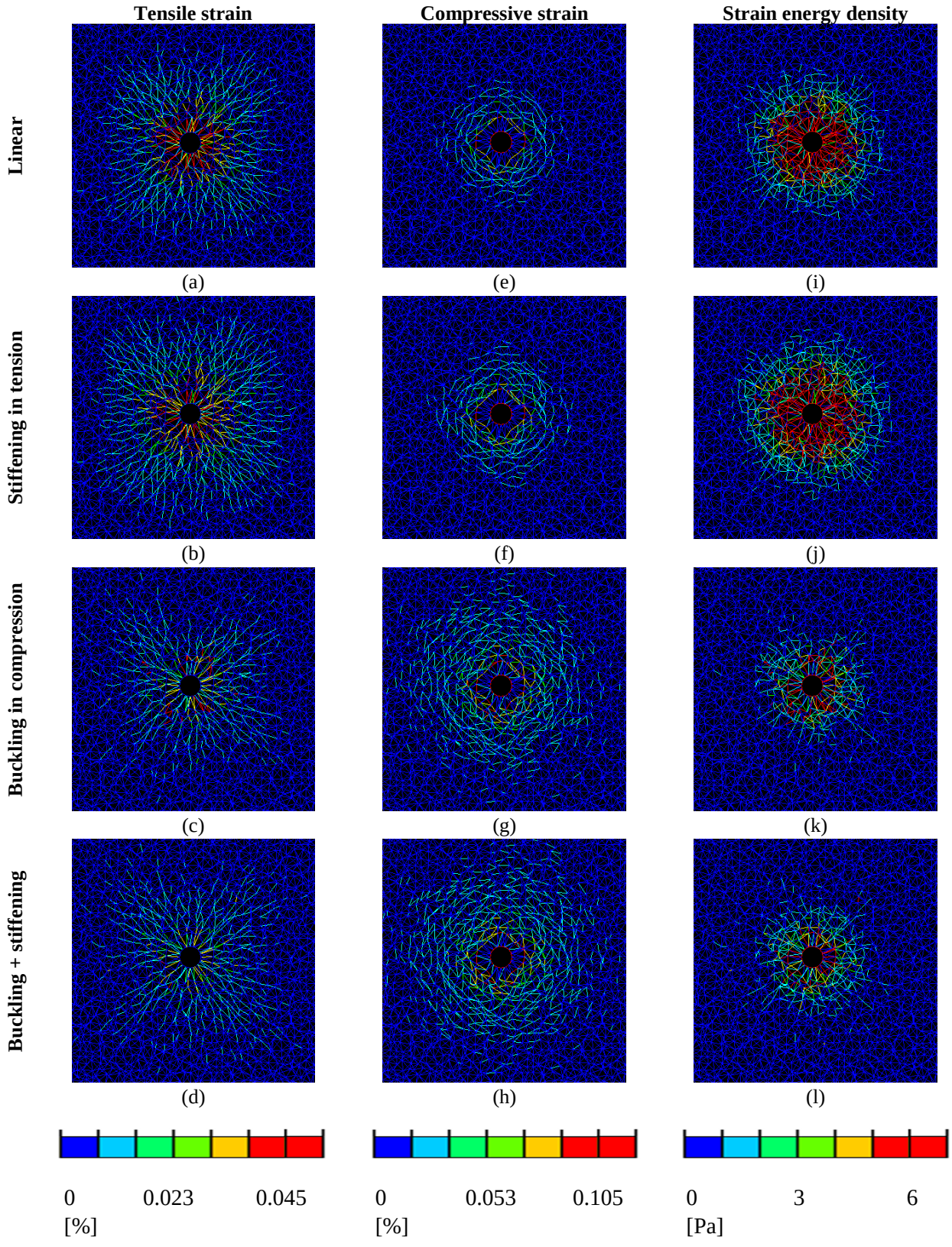

Figure S4: Tensile (logarithmic) strains (left column), compressive (logarithmic) strains (middle column) and SEDs (right column) occurring in the fiber segments within the vicinity of a single, isolated contracting cell, for 25% contraction. Plots were produced for all four material models used to simulate the mechanical behavior of the individual fibers (**Error! Reference source not found.**c).

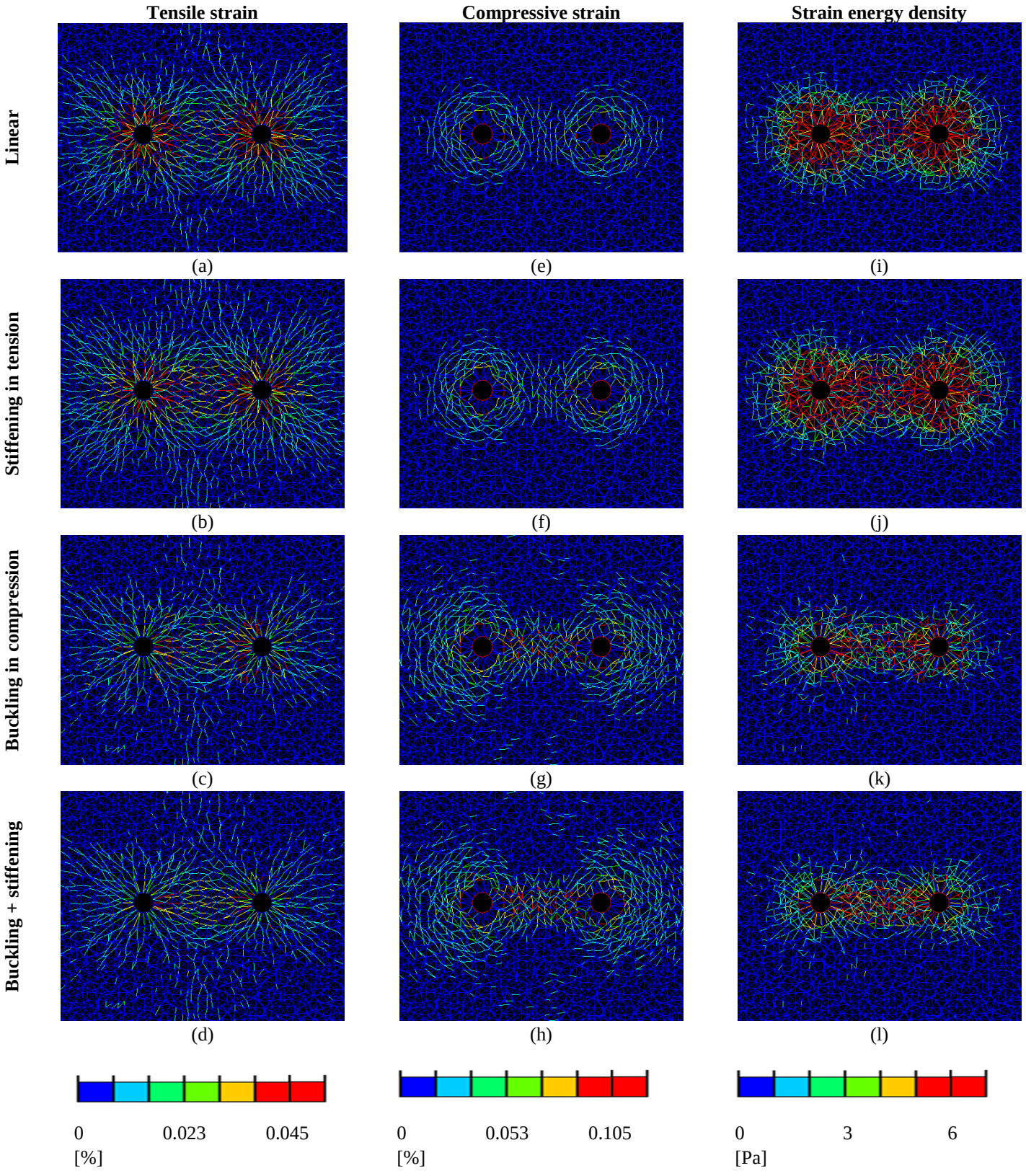

Figure S5: Tensile strains (left column), compressive strains (middle column) and SEDs (right column) occurring in the fiber segments within the vicinity of two neighboring contracting cells (here the cell-to-cell distance is 3.4 cell diameters as an example), for 25% contraction. Plots were produced for all four material models used to simulate the mechanical behavior of the individual fibers (**Error! Reference source not found.**c).

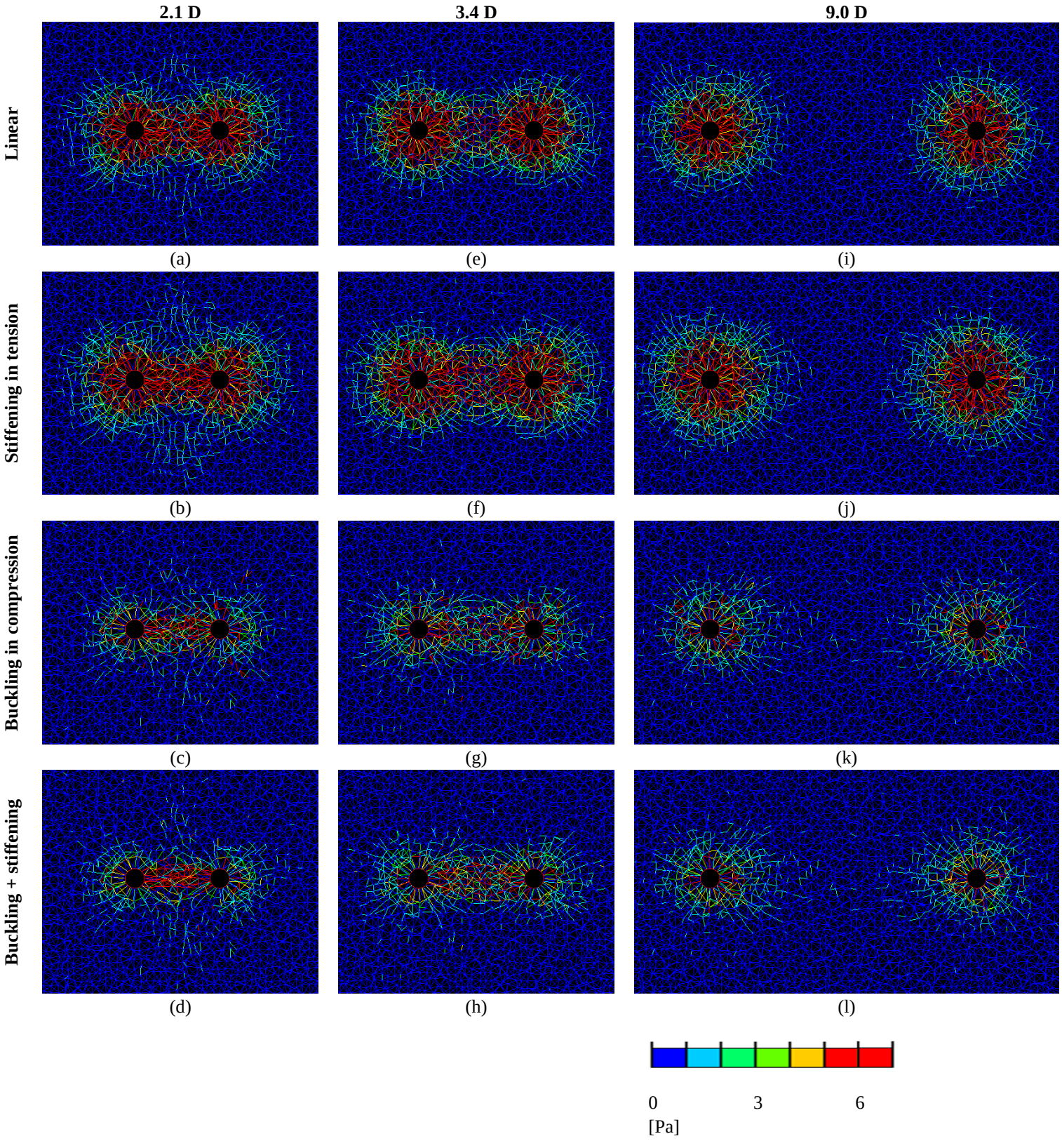

Figure S6: SEDs occurring in the ECM fiber segments surrounding two contracting cells located at various distances, for 25% contraction. Cell-to-cell distances shown here are 2.1 (left column), 3.4 (middle column) and 9.0 (right column) cell diameters. Plots were produced for all four material models used to simulate the mechanical behavior of the individual fibers (**Error! Reference source not found.**c).

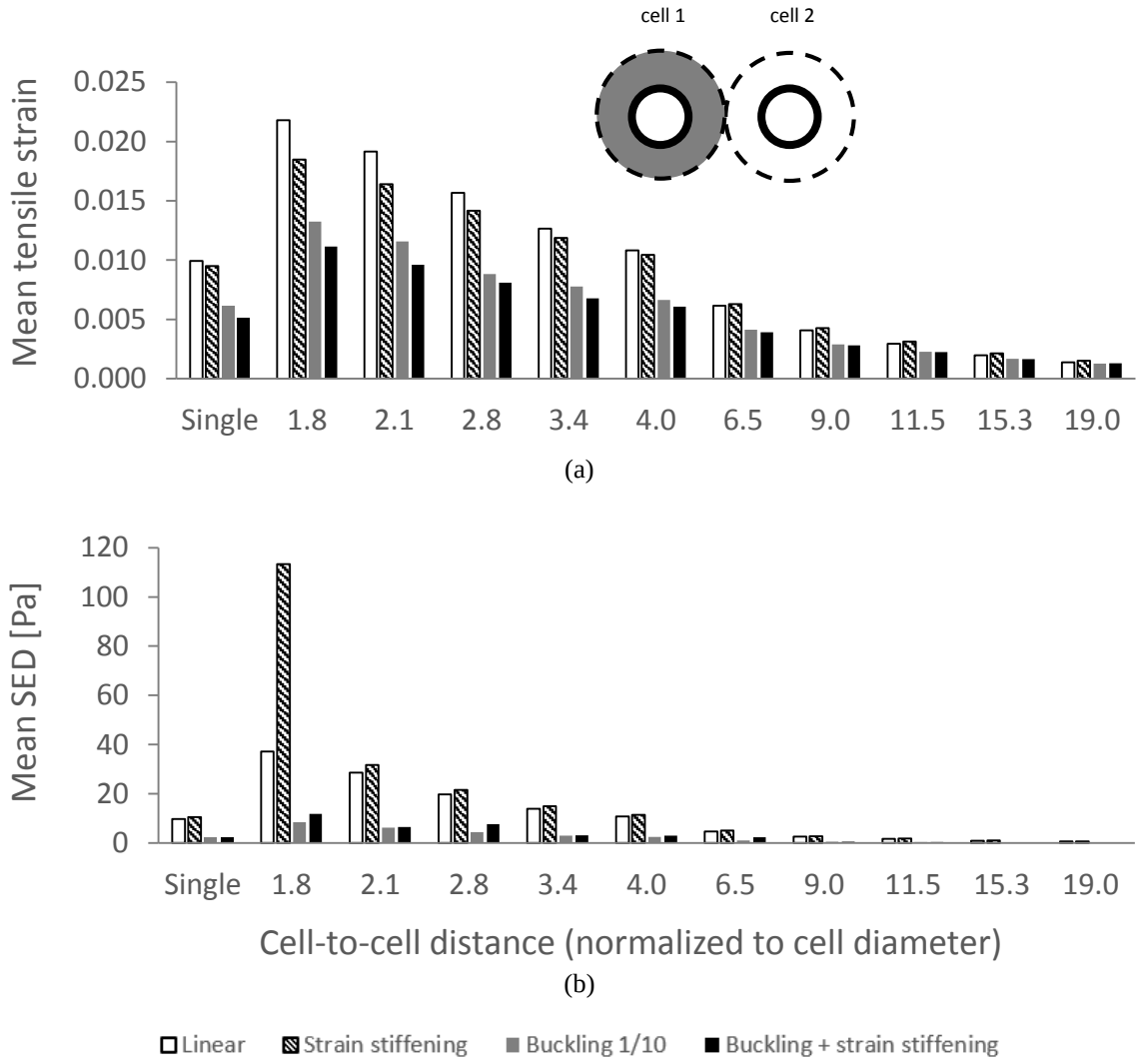

Figure S7: Mean tensile (logarithmic) strain (a) and SED (b) occurring within a disc surrounding an individual cell, of radius equals to half of the cell-to-cell distance, for 25% contraction. The model variants shown include several cell-to-cell distances (in terms of cell diameter, D) and all four material models used to simulate the mechanical behavior of the individual fibers (**Error! Reference source not found.**c). The values calculated for the single-cell model variants (assuming a disc of radius equals to half of the cell-to-cell distance of 2 cell diameters) are shown for comparison.

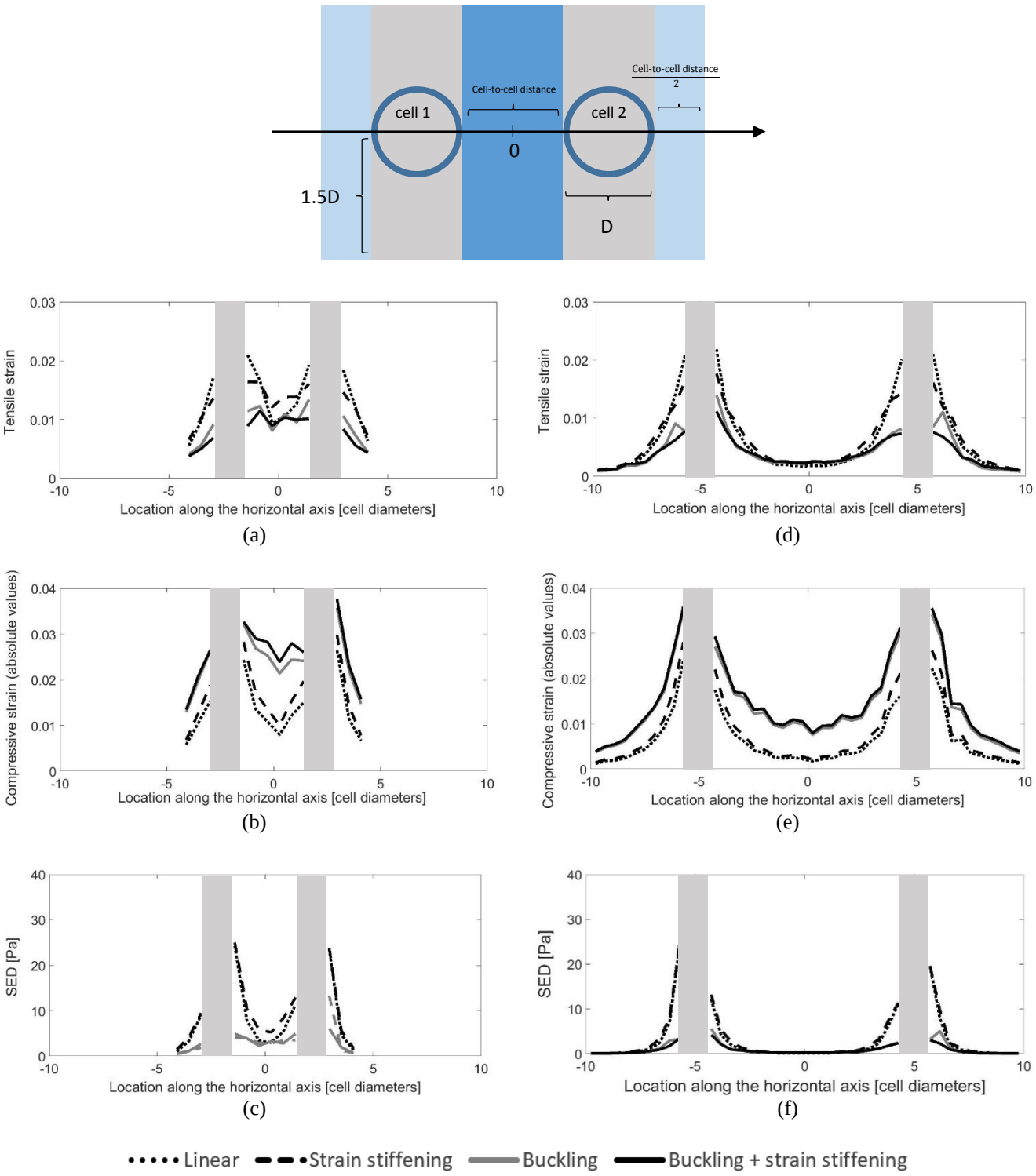

Figure S8: Tensile strains, compressive strains and SEDs occurring within the inter-cellular band and the opposite ECM regions. Loads occurring in the ECM fibers falling within the inter-cellular band (a rectangular-shaped area containing the line connecting the centers of the two contracting cells, with length equaling the inter-cellular distance and width equivalent to 3 cell diameters; blue area in the top panel) and within the opposite areas of the matrix (two sky-blue areas in the top panel) were averaged and plotted along a horizontal line, for 25% cell contraction, four types of fiber mechanical behavior (**Error! Reference source not found.**c) and two example cell-to-cell distances (3.4 cell diameters, left column, and 9.0 cell diameters, right column). Gray rectangles indicate the areas occupied by the cells themselves.

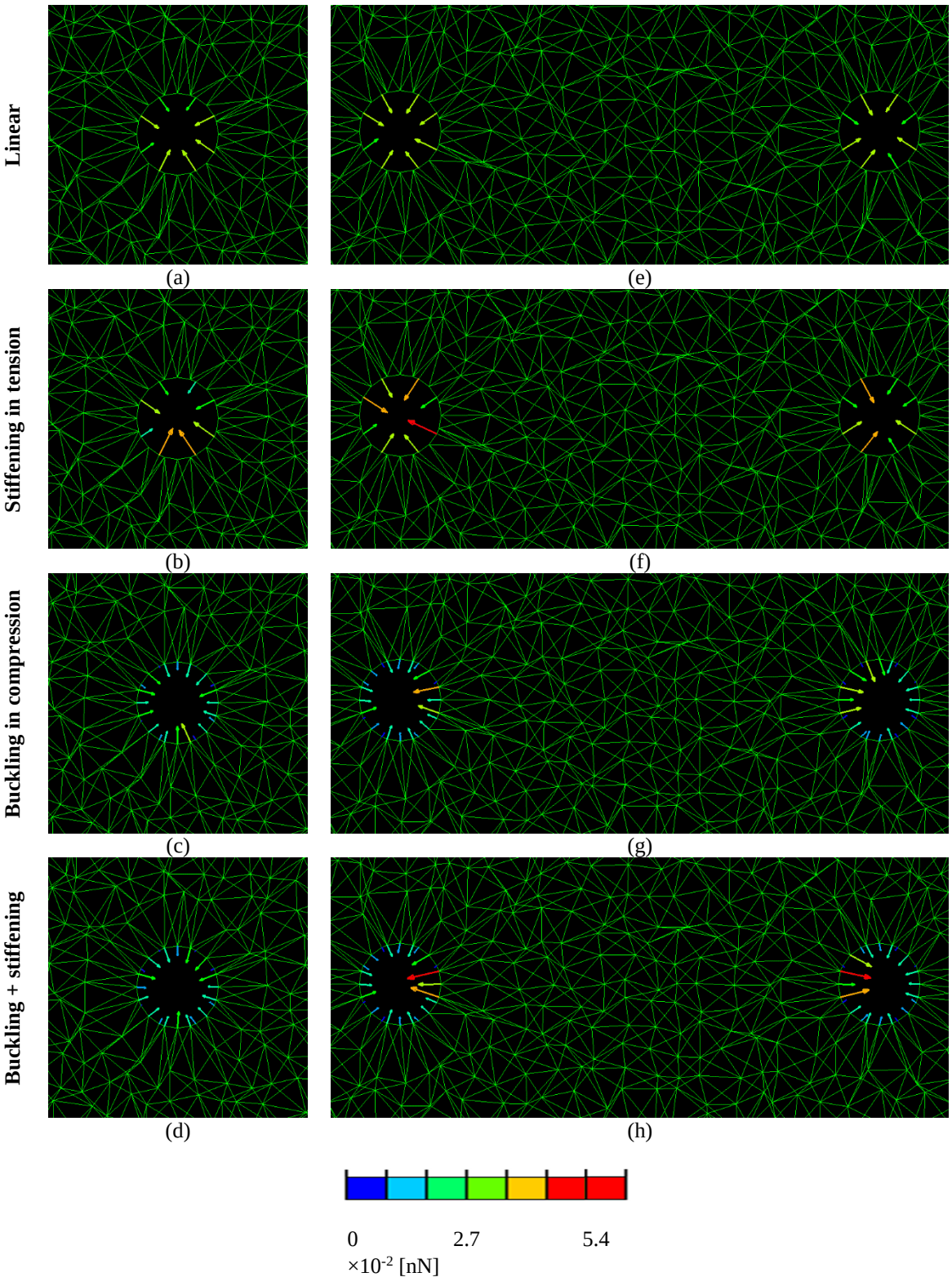

Figure S9: Reaction forces occurring on the cell boundaries for a single (left column) or two (right column; here distance between the neighboring cells is 3.4 cell diameters as an example) contracting cells, for 25% contraction. Plots were produced for all four material models used to simulate the mechanical behavior of the individual fibers (**Error! Reference source not found.**c).

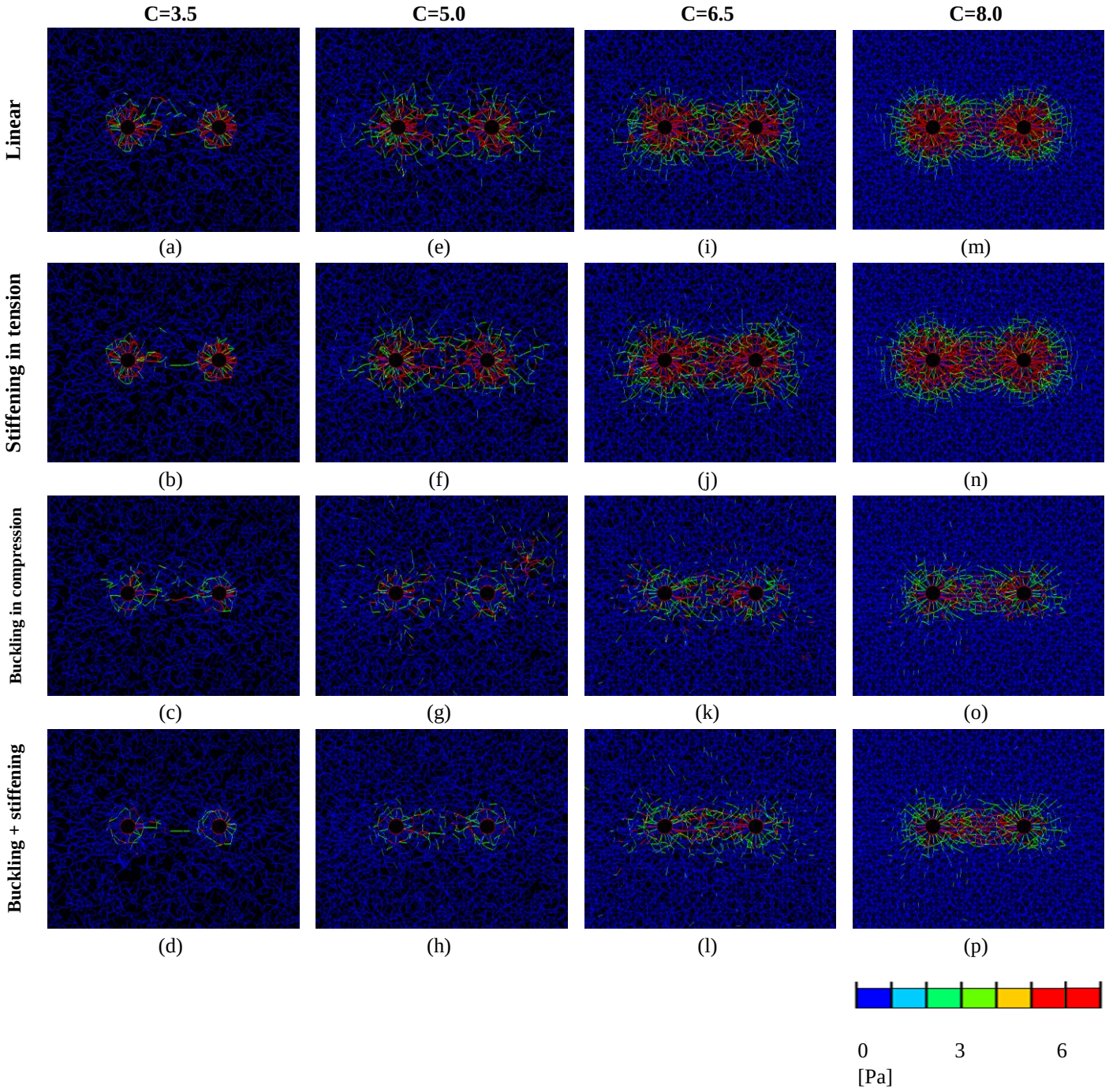

Figure S10: Effect of network connectivity. SEDs occurring in the fiber segments around two neighboring contracting cells (here the cell-to-cell distance is 3.4 cell diameters as an example), for 25% contraction and four levels of network connectivity (C=3.5, 5.0, 6.5, 8.0). Plots were produced for all four material models used to simulate the mechanical behavior of the individual fibers (**Error! Reference source not found.**c).

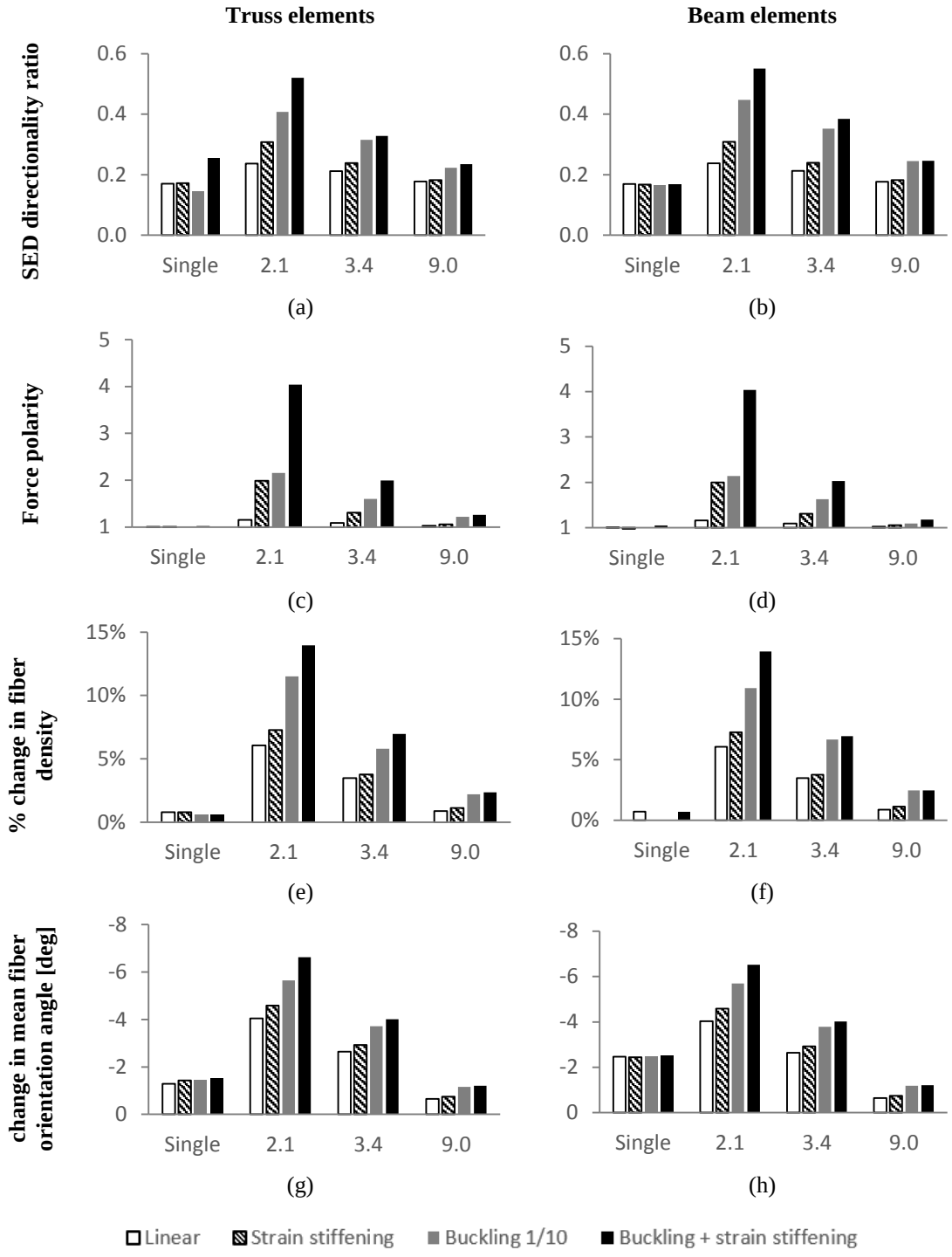

Figure S11: Bar charts demonstrating the effects of element selection (truss/beam) on the SED directionality ratio (a and b), force polarity on the cell boundaries (c and d) and change in fiber density (e and f) and orientation (g and h) within the inter-cellular region of the matrix, for 25% cell contraction, for four material models, a single cell and cell-to-cell distances of 2.1, 3.4 and 9.0 cell diameters.

The effect of mean fiber length on the model outcomes - Figure S12

In order to account for potential biological variability of the cell sizes and network fiber lengths, and to investigate the effects of the cell diameter / mean fiber length ratio on the model outcomes, we conducted a sensitivity analysis. We thus modified the mean fiber length from 3.5 to 7.0 μm (while keeping the cell diameter constant). The trends reported herein – namely the contribution of fiber nonlinear elastic behavior to enhancing the directionality of loads and structural remodeling of the inter-cellular ECM– were valid for the increased mean fiber length. Also, most outcome measures reached plateaus at cell-to-cell distances above 9 cell diameters, similarly to the shorter fiber-length case, indicating that mechanical interaction no longer exists (Figure S12).

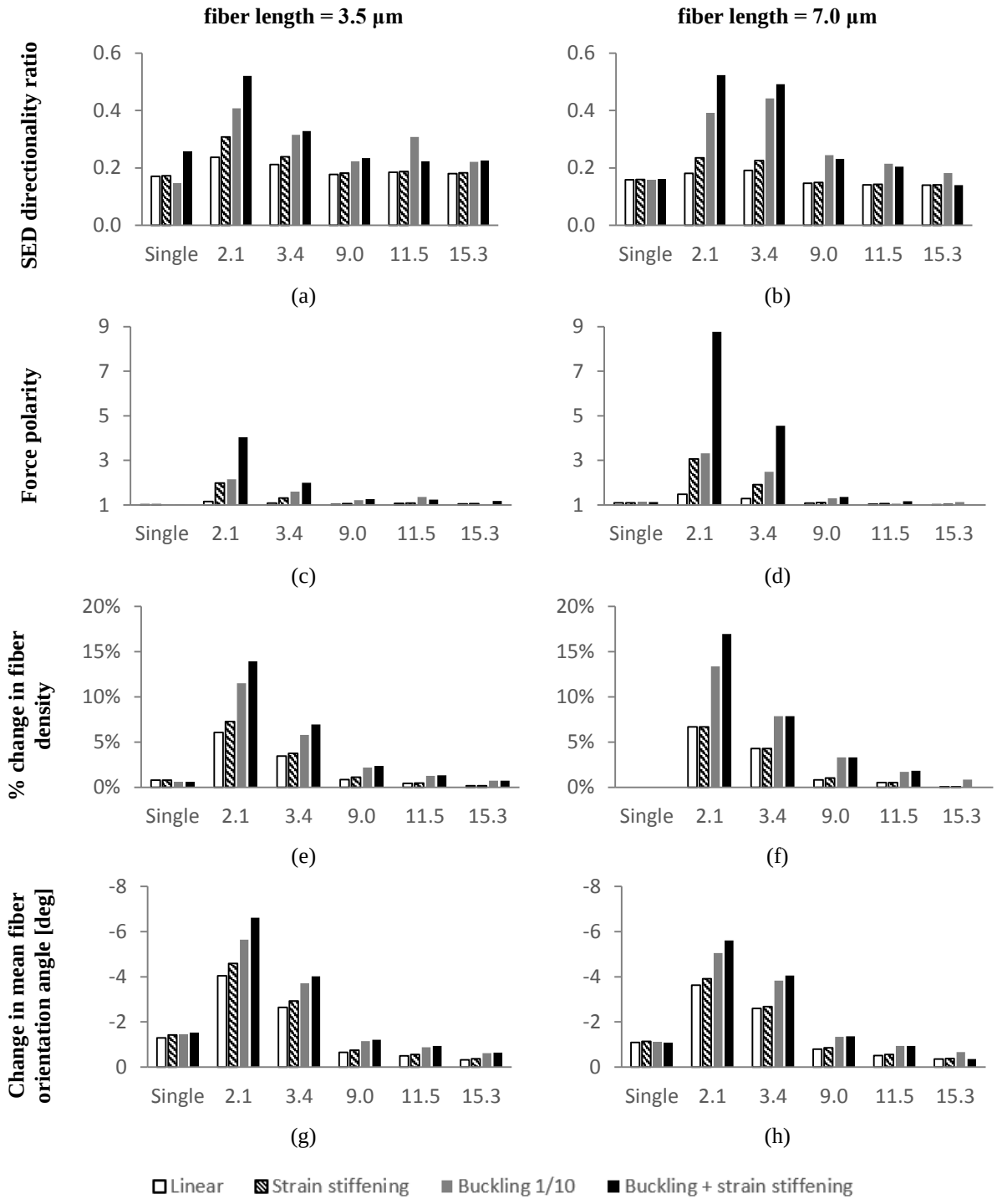

Figure S12: Bar charts demonstrating the effects of mean fiber length on the SED directionality ratio (a and b), force polarity on the cell boundaries (c and d) and change in fiber density (e and f) and orientation (g and h) within the inter-cellular region of the matrix, for 25% cell contraction, for four material models, a single cell and cell-to-cell distances of 2.1, 3.4, 9.0, 11.5 and 15.3 cell diameters.